



OPEN

Investigation of SARS-CoV-2 inactivation using UV-C LEDs in public environments via ray-tracing simulation

Po-Yen Lai¹✉, Huizhe Liu¹, Ray Jia Hong Ng¹, Bianca Wint Hnin Thet¹, Hong-Son Chu¹, Jin Wah Ronnie Teo², Qunxiang Ong³, Yuanjie Liu⁴ & Ching Eng Png¹

This paper proposes an investigating SARS-CoV-2 inactivation on surfaces with UV-C LED irradiation using our in-house-developed ray-tracing simulator. The results are benchmarked with experiments and Zemax OpticStudio commercial software simulation to demonstrate our simulator's easy accessibility and high reliability. The tool can input the radiant profile of the flexible LED source and accurately yield the irradiance distribution emitted from an LED-based system in 3D environments. The UV-C operating space can be divided into the safe, buffer, and germicidal zones for setting up a UV-C LED system. Based on the published measurement data, the level of SARS-CoV-2 inactivation has been defined as a function of UV-C irradiation. A realistic case of public space, i.e., a food court in Singapore, has been numerically investigated to demonstrate the relative impact of environmental UV-C attenuation on the SARS-CoV-2 inactivation. We optimise a specific UV-C LED germicidal system and its corresponding exposure time according to the simulation results. These ray-tracing-based simulations provide a useful guideline for safe deployment and efficient design for germicidal UV-C LED technology.

Coronavirus disease 2019 (COVID-19), caused by severe acute respiratory syndrome coronavirus 2 (SARS-CoV-2), was first detected in December 2019 in Wuhan, China, and has since sparked a global pandemic. A respiratory infection such as SARS-CoV-2 can be transmitted from direct physical contact with the virus from an infected person's respiratory fluids or via droplets on surfaces and aerosol transmission^{1,2}. As a consequence, internationally coordinated efforts have been put into large-scale medical, scientific, economic, and public undertakings to prevent fomite transmission, particularly for high touch surfaces in public environments³.

Existing surface disinfection approaches such as chemical spraying⁴, thermal treatment⁵, or surface wiping can be labor-intensive, costly, and consumes high energy. Therefore, it is imperative to develop a safe and effective non-contact sanitising solution to prevent fomite transmission in public spaces. Light-based inactivation using Ultraviolet-C (UV-C) light sources ($220 < \lambda < 280$ nm) has been proven to be one of the most efficient ways of inactivating a wide range of microbes and viruses by destroying their DNAs or RNAs, including SARS-CoV-2^{6,7}. While germicidal UV-C Mercury (Hg) lamp is widely used in water treatment and air handling units⁸, the directionality of LED offers a more targeted and safer alternative compared to the Hg lamp. It also exhibits several advantageous features such as environmental friendliness, energy savings, compact size, low cost, and durability⁹. The inactivation of SARS-CoV-2 using UV-C LED also becomes a significant concern for its practical importance in mitigating COVID-19 transmission. The works^{10,11} performed the study for the reduction of airborne SARS-CoV-2 spread using far-UV-C ($\lambda = 222$ nm) LEDs. Similarly, several articles^{12–14} showed that the LEDs within a UV-C range ($265 < \lambda < 280$ nm) are the promising light source to inactivate SARS-CoV-2 by photo-degradation of spike protein rapidly. Moreover, Liu et al.¹⁵ proposed the AlGaIn-based LEDs ($\lambda = 275$ nm) structure design and epitaxy optimisation for achieving a fast inactivation of SARS-CoV-2 using high-power UV-C irradiation. However, one major drawback of UV-C germicidal irradiation is its harmful effect on human eyes and skin, so that there are international safety guidelines to limit human exposure^{16,17}.

¹A*STAR Institute of High Performance Computing, Electronics and Photonics, 1 Fusionopolis Way, #16-16, Connexis 138632, Singapore. ²A*STAR Singapore Institute of Manufacturing Technology, 2 Fusionopolis Way, #08-04, Innovis 138634, Singapore. ³A*STAR Singapore Bioimaging Consortium, 11 Biopolis Way, #02-02, Helios 138667, Singapore. ⁴A*STAR National Metrology Centre, 2 Fusionopolis Way, #08-05, Innovis 138634, Singapore. ✉email: lai_po-yen@ihpc.a-star.edu.sg

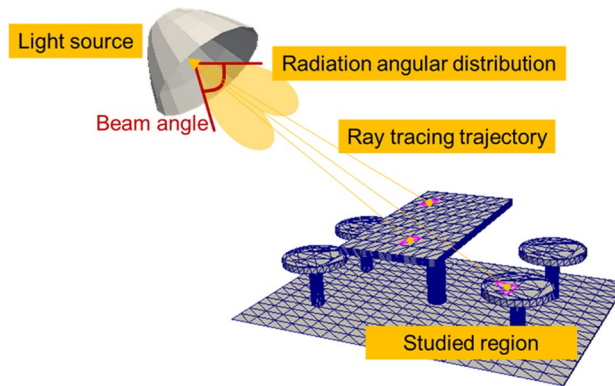


Figure 1. Schematic illustration of the RT model to predict the radiation level in the area of interest.

Optical simulations can readily guide not only the efficient design of germicidal UV-C LED but implementation of safe deployment which is particularly important as UV-C wavelength is not visible to naked human eyes. Currently, there are only a few numerical systematic studies^{10,10} on UV-C radiation mapping in public environments. The work¹⁰ proposed a coupled-CFD radiative model for predicting airborne SARS-CoV-2 inactivation in a single-occupancy private room in hospitals, a simplified 2D system in simulations. Another recent work by Hou et al.¹⁸ conducted a parametric study of UV-C germicidal technology in a patient room in hospitals by adjusting the room configuration, ceiling height, and surface materials using ray-tracing simulation. Apart from the proposed numerical works^{10,10} for evaluating the UV-C germicidal effectiveness in medical facilities, the simulation demonstrations on three-dimensional (3D) UV-C mapping in environments of day-to-day life are still lacking. In addition, the systematic study of both UV-C LEDs in inactivation on surfaces of the complex 3D environments and the margin of safety for UV-C LEDs are indispensable during the COVID-19 pandemic.

In this work, we develop an in-house ray-tracing (RT) simulator based on UV-C LEDs to inactivate SARS-CoV-2 in public environments. Based on a physically accurate and geometrically flexible RT, our proposed simulator can model the specific design of a UV-C LED array and generate the corresponding irradiance map in a large-scale ambient operating environment. The simulated irradiance map guides a defined safe boundary with a designated inactivation zone during the germicidal operation. Furthermore, these RT simulations help optimise the light source's distance and determine the exposure time for a sufficient UV-C dose. In addition, environmental UV-C attenuations^{7,19} due to superficial dirt and substances in the air have been summarized as compact mathematical forms and considered in the RT simulator. The methodology of this work, including the RT model, the experimental setup for benchmark, and the quantitative determination of SARS-CoV-2 inactivation, is described in “Methods” section. The case study of a public environment based on 3D RT simulations and the parametric analysis considering ambient environmental attenuations is presented in the following section. Finally, the discussion, concluding remarks, and outlook on the work are given.

Methods

UV-C LED radiation model. In this section, we proposed an RT model to predict the UV-C radiation level in the area of interest. The model is developed based on the RT technique that is physically accurate, highly flexible with geometrical input, and easy to parallelize. In Fig. 1, the light source is defined by its structure (e.g., single LED or LED array) and amplitude spatial distribution, including the beam angle and radiation angular distribution. Next, the complex studied region is geometrically described in STereoLithography (STL) format, in which uniform triangle meshes are automatically generated for a suitable mesh resolution. Finally, the backward RT technique is applied to trace the rays from each mesh point to the light source.

The irradiance ϕ [W/m²] in the far-field can be expressed as a function of radiant intensity $I(\theta)$ [W/sr], in which θ is a polar angle in a coordinate system centered in the emission source²⁰, given by

$$\phi = \frac{I(\theta)\cos\theta_d}{r^2}, \quad (1)$$

where θ_d the incident angle to the detector mesh point, and r is the distance between the source and the detector. The total irradiance on a detector from a given UV-C LED module consists of N point sources (i.e., LEDs) at an operating wavelength λ_0 with total power P_{s,λ_0} can be re-written as

$$\phi_{d,\lambda_0} = \frac{P_{s,\lambda_0}/N}{2\pi \int_{-\pi/2}^{\pi/2} I_{n,\lambda_0}(\theta_s) \sin\theta_s d\theta_s} \sum_N \frac{I_{n,\lambda_0}(\theta_s) \cos\theta_d}{(x_s - x_d)^2 + (y_s - y_d)^2 + (z_s - z_d)^2}, \quad (2)$$

where $I_{n,\lambda_0}(\theta_s)$ is the normalized radiant intensity, also called the angular radiant distribution, and θ_s is the polar angle in a coordinate system centered in the point source. The coordinates (x_s, y_s, z_s) and (x_d, y_d, z_d) are the light source positions and the detector mesh point, respectively. From Eq. (2), the information about the distances between the LEDs in the LED module is included in the summation of all the sources, as the different LED

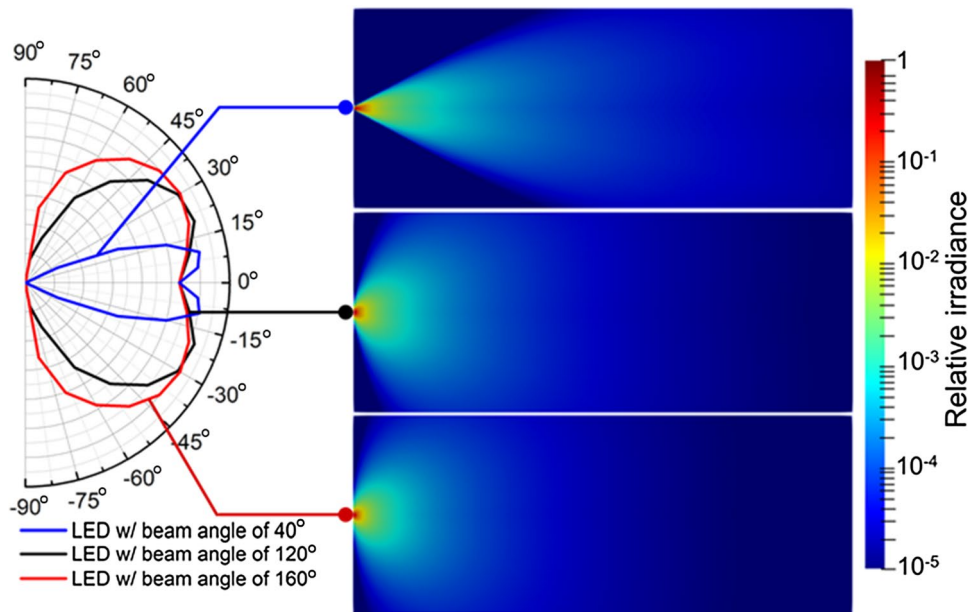


Figure 2. Radiation angular profile and irradiance of UV LED with the beam angle of 40°, 120°, and 160°, respectively.

sources will have different spatial coordinates (x_s, y_s, z_s), as well as different angles θ_s and θ_d , giving different values for the integrand in the calculation of the irradiance for the respective sources.

Figure 2 shows the irradiance distributions on 2D cut-planes predicted by the RT model where the light sources are the single LED with a beam angle of 40°, 120°, and 160°, respectively. In the left panel of Fig. 2, these Lambertian-like radiation profiles²⁰ are the common types of UV-C LED for sterilization²¹ which gives the angular radiant distribution $I_{n,\lambda_0}(\theta_s)$ in Eq. (2). The corresponding cut-plane irradiance distribution, calculated from Eq. (2), varies as the beam angle is changed. Each LED is assumed as a point source with a given radiation profile based on the far-field approximation in this work. In this case, it is convenient to demonstrate the design of an LED array using the linear superposition of the irradiance from different single LEDs.

Model validation. Figure 3 shows the experimental setup for measuring the radiation profile of the UV-C LED light source. The upper picture in Fig. 3a shows the UV-C LED strip light source consisting of a linear arrangement of 25 single LEDs spaced 0.005 m apart with a measured total power of 0.194 W and a peak wavelength of ~274 nm. The middle picture in Fig. 3a presents the measurement setup of the UV-C light source. The light source under test is attached to a rotatable holder of a goniometer to measure the spatial light distribution at a distance of 1.5 m apart. The UV-C irradiation measurement setup is calibrated and validated using standards traceable to The International System of Units (SI). As shown in the schematic illustration at the bottom of Fig. 3a, the light source-under-test can be rotated around the c -axis and γ -axis of the spectrometer, and the irradiance at the detector is recorded. The c -axis is perpendicular to the LED strip's luminous surface, and the light source is rotated at 15° intervals between $0^\circ \leq c \leq 345^\circ$. At each c angle, the light source is rotated about the γ axis parallel to the light source's luminous surface under test at 10° intervals between $0^\circ \leq \gamma \leq 70^\circ$. To validate the RT model, Fig. 3b shows the model predictions of peak irradiance at different distances to the light source and compares it to the experimental measurement. There is a good agreement between them. For the sake of simplicity, the detected radiant profile is averaged out over the c -axis, and this averaged angular distribution (see the inset in Fig. 3b) is defined as the input angular radiation profile for the LED light source. Figure 3b also shows the comparison between results simulated using the in-house-developed RT solver and the commercial software, Zemax OpticStudio²². They are well agreed for a given input angular radiation profile.

Inactivation coefficient of SARS-CoV-2. While SARS-CoV-2 is exposed to UV-C light, the viral concentration decays exponentially as a function of time and the UV-C dosage. The experimental data are well described by the relation¹²:

$$S = 1 - e^{-KD}, \quad (3)$$

where S and D represent the sterilizing rate of SARS-CoV-2 and the UV-C dose (in the unit of J/m^2) at the target surface.

K is a factor called the inactivation coefficient that can be estimated from the survivorship curves by fitting the experimental data¹². Figure 4 shows $K^{11,12}$ as a function of exposure wavelength at 222 nm, 265 nm, 280 nm, and 300 nm, respectively. The trend of K is close to the germicidal effectiveness provided by Deutsches Institut für Normung (DIN)²³ and Illuminating Engineering Society of North America (IESNA)²⁴. To evaluate the

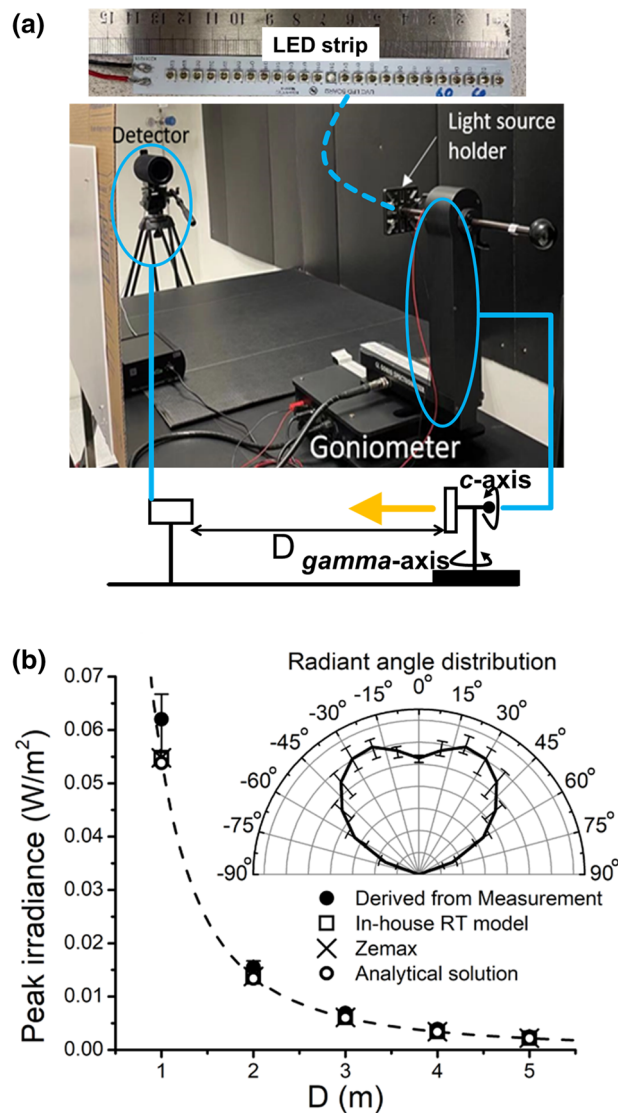


Figure 3. (a) The picture of the experimental setup and the schematic illustration for measuring the radiation emitted by LED strips are shown. (b) The model validation by comparing the peak irradiance derived from the measurement and the simulation done by the in-house-developed RT model, Zemax OpticStudio, and the analytical solution. The inset in (b) shows the angular radiation pattern of a single LED. The error bars comes from the standard deviation of the average in c angles.

effectiveness of SARS-CoV-2 inactivation on the operating wavelength at 274 nm, we suppose the corresponding value of K using linear interpolation based on the experimental data^{11,12}. K values at 222 nm and 274 nm are close to 4.1 where the K value for 222 nm is directly obtained from the experiment¹¹ and the K value for 274 nm is estimated from the linear interpolation.

By considering the radiative attenuation effect in practical environments, the general expression of the UV-C dose D at distance r from the light source during the exposure time τ can be expressed as

$$D = (1 - \eta)e^{-\alpha r} \phi(r)\tau, \quad (4)$$

where $\phi(r)$, η , and α respectively represent the UV-C intensity at the target surface, the attenuation factor due to the surface moisture and dirt, and the extinction coefficient due to the radiative loss in a medium. $\phi(r)$ can be numerically calculated using the RT model. For the sake of simplicity, η and α are assumed as constants of r and τ that are given values for certain conditions.

Results

In this section, we perform a numerical study for the UV-C sterilization dosage using a specific-designed LED germicidal system in a typical Singapore food court. It is one of the important common public spaces in Singapore, which is an integral part of the way of life for Singaporeans, where people from all walks of life gather at food court centres to dine and bond over their favourite food. In the following simulations, open boundary

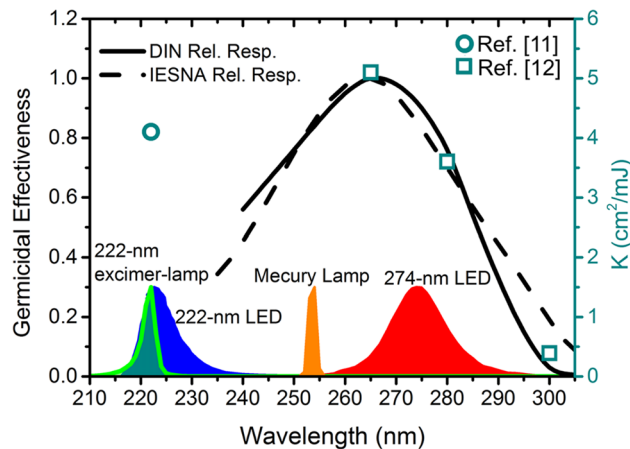


Figure 4. The germicidal effectiveness provided by Deutsches Institut für Normung (DIN)²³ and Illuminating Engineering Society of North America (IESNA)²⁴, and SARS-CoV-2 inactivation coefficient K versus radiation wavelength in which the scatter points achieved from the experiments^{11,12}. The typical spectra of excimer lamp (luminous green line), UV-C LEDs (blue for 222-nm and red for 274-nm), and mercury lamp (orange) are shown at the bottom of the figure.

conditions are adopted excepted for the ground because the distances from the area of concern to the walls and ceil are > 5 times of R_{eff} . The UV-C reflections from the surface of the food court are neglected due to of commonly found materials (e.g., PVC²⁵ and ceramic tiles²⁶) in a food court and a doubled optical path (i.e., the inverse-square law of light).

Case study of a typical food court in Singapore. The configuration of a germicidal system designed with an array of 3×6 UV LED strips is illustrated in Fig. 5a. The UV-C LED germicidal system can be handheld or mounted onto a mobile robot. In the upper panel of Fig. 5a, the UV LED strips are embedded in the LED carrier. Two vertical slices of the calculated radiation pattern emitted from the LED array are shown in the lower panel of Fig. 5a. Depending on the emitted irradiance level, the exposure space is divided into the effective germicidal zone with emitted irradiance of $> 18.7 \mu\text{W}/\text{cm}^2$ for which a 90% inactivation of SARS-CoV-2 can be achieved within half a minute, the safe zone with emitted irradiance of $< 0.1 \mu\text{W}/\text{cm}^2$ according to international guidelines^{16,17,27}, and the buffer zone in between. For the effective germicidal purpose, Fig. 5b shows the radius (i.e., R_{eff}) of the zone along with the distance (i.e., H) from the center of the LED array under LEDs with different beam angles. R_{eff} increases with H increased until R_{eff} reaches the maximum value. R_{eff} is proportional to the beam angle of the composed LEDs for the small values of H . However, the array composed of LEDs with a beam angle of 120° exhibits the largest R_{eff} among the three cases due to the specific design of the array, as shown in Fig. 5a. Moreover, the volume of the germicidal zone reaches the maximum while H is around 1.1.

Figure 6a shows a schematic of a typical table setting configuration in a public food court where the LED array is located in the center of the space with a distance of 1.1 m from the ground. The color mapping on the surface of the food court represents the zones at different UV-C irradiance levels as defined in Fig. 5a. According to the initial conditions, the simulated 3D UV-C irradiation mapping on the food court surface with a 30-s exposure time is shown in Fig. 6b. The value of irradiation is calculated from the time integration of emitted irradiance of the LED array, where the wavelength of the LED is 274 nm. The region near the LED array has higher UV-C irradiation. Otherwise, the regions far from the LED array, where the angle from the LED is large, and behind obstacles have a relatively low UV-C irradiation. Ignoring the radiative extinction due to the attenuation from the surface and the light path; i.e., $\eta = 0$ and $\alpha = 0$ in Eq. (4), the inactivation of the food court (see Fig. 6c) can be calculated using Eq. (3). Here the inactivation coefficient is set to 0.41, which is the value that corresponds to the wavelength of 274 nm (see Fig. 4). In addition, since the inactivation coefficient for the wavelength of 222 nm is also around 0.41, the activation map for 222 nm would be identical to that in Fig. 6c, assuming that the spatial radiative distribution of the LED's and arrangement of the LED array remain the same. Figure 6c shows that the distribution of inactivation is consistent with the zone map shown in Fig. 6a, as expected.

Parametric analysis of the exposure time for sterilization. To evaluate the exposure time for sterilization, Fig. 7a shows the ratio of the area A_{ster} with the specific disinfection level to the UV-C exposed area A_{ex} varying with the exposure time. The ratio parameter $A_{\text{ster}}/A_{\text{ex}}$ increases asymptotically with the exposure time t_{ex} from zero to a saturation point with an approximate value of 0.71. The saturation point is defined as the value of $A_{\text{ster}}/A_{\text{ex}}$ at which the rate of rising in $A_{\text{ster}}/A_{\text{ex}}$ is $< 5\%$ of the maximum rate of rising in the initial stage. The required time for the UV-C exposure to saturation is defined as τ_{sat} . As the inactivation level increases, the LED array has a higher requirement of τ_{sat} . For the usual viral inactivation (i.e., 3-log), τ_{sat} has to be > 10 min. τ_{sat} becomes > 20 min if the higher viral inactivation of 5-log is required. Figure 7b summarizes the values of τ_{sat} for different inactivation levels for the ideal case and when considering surface attenuation (i.e., $\eta = 0.1$). The

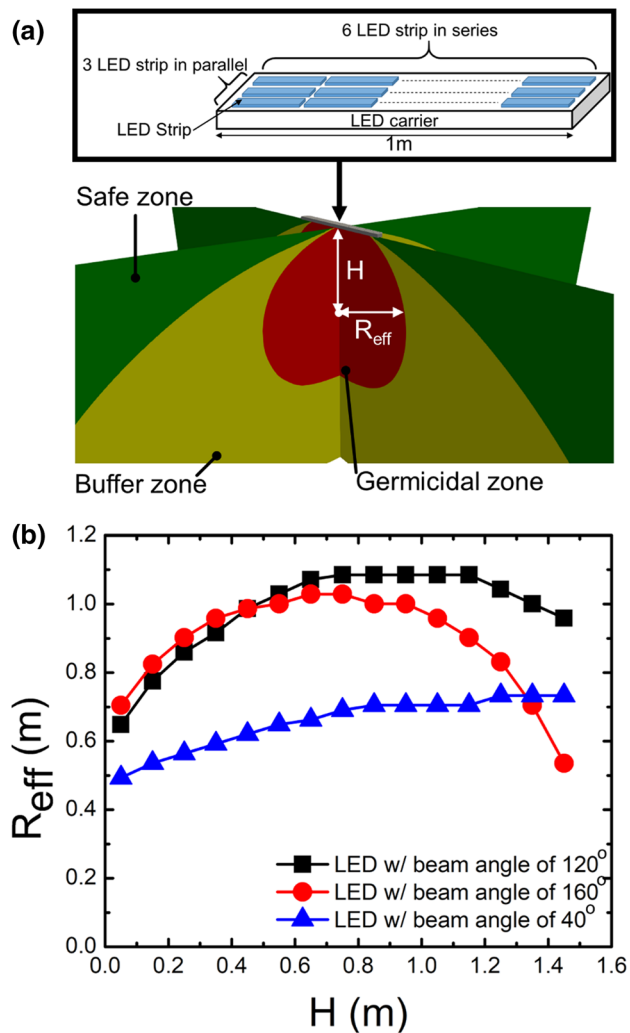


Figure 5. (a) The germicidal system designed with LED array composed of 3×6 LED strips is shown in the upper panel. The lower panel shows the vertical slice views of irradiation pattern emitted from the LED array in which the space can be divided into the safe zone in green (i.e., $< 0.1 \mu\text{W}/\text{cm}^2$), the buffer zone in yellow, and the effective zone in red (i.e., $> 18.7 \mu\text{W}/\text{cm}^2$). R_{eff} is the radius for the effective germicidal region, for a particular distance H between the LED array and the detection point. (b) The correlation between H and R_{eff} at the beam angle of 120° , 160° , and 40° .

surface attenuation of UV-C radiation increases the required τ_{sat} for all inactivation levels. The increment of τ_{sat} is proportional to the τ_{sat} itself for the specific inactivation level due to the linear approximation in Eq. (4).

Each ray travels through intermediate substances in a straight path before it hits the target surface in the RT model. The substances may absorb and scatter the UV-C ray, and the radiant energy is attenuated along the light path. In this case, the extinction coefficient α may not be 0 in Eq. (4). Figure 8a shows the light extinction effect on the relationship between $A_{\text{ster}}/A_{\text{ex}}$ and the corresponding exposure time. Ideally, $A_{\text{ster}}/A_{\text{ex}}$ will attain saturation after 12.5-min of UV-C exposure. When $\alpha = 0.6$, τ_{sat} will substantially increase to almost four times the original value. Figure 8b reveals the dependence of τ_{sat} versus α in which τ_{sat} increases significantly as α increases.

Discussion

In Fig. 5a, the radiant characteristics of the specific-designed LED array are simulated using the RT model. We can evaluate the corresponding inactivation level from Eq. (3). According to the calculated UV-C intensity pattern in space, we divide the exposure region into the effective, buffer, and safe zones, respectively. To maximize the area for the effective UV-C germicide using the LED array, the intrinsic beam angle of a single LED is 120° and the distance to the ground is ~ 1.1 m, as revealed by Fig. 5b. It is worth noting that the optimised values of beam angle and distance to the ground apply to the specific design of the LED array, as presented in Fig. 5. In Fig. 6, we perform a case study of UV-C sterilization in a public environment using the RT model. In Fig. 6a, we differentiate the UV-C exposed surfaces of the food court into specific zones defined in Fig. 5a. From the simulated 3D irradiation in Fig. 6b and the calculated inactivation map in Fig. 6c, we define the parameter τ_{sat} , which is the required time for the effective sterilization in the UV-C irradiation region. This parameter

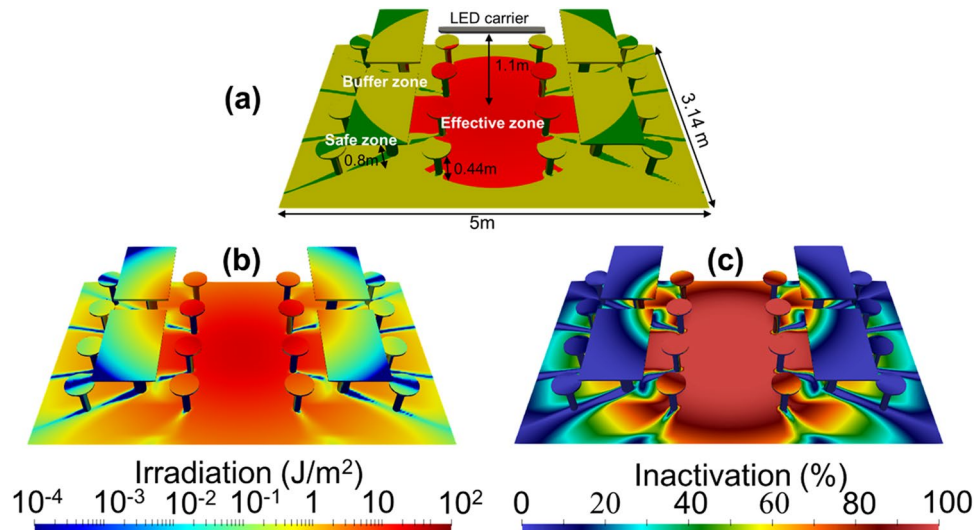


Figure 6. (a) The schematic feature of a typical food court in Singapore where the LED array (shown in Fig. 5a) is located in the center of the food court and 1.1-m from the ground. The zone map is defined (b) 3D irradiation mapping of the food court after a 30-s UV-C exposure, and the corresponding inactivation of SARS-CoV-2 evaluated from Eq. (3) is shown in (c).

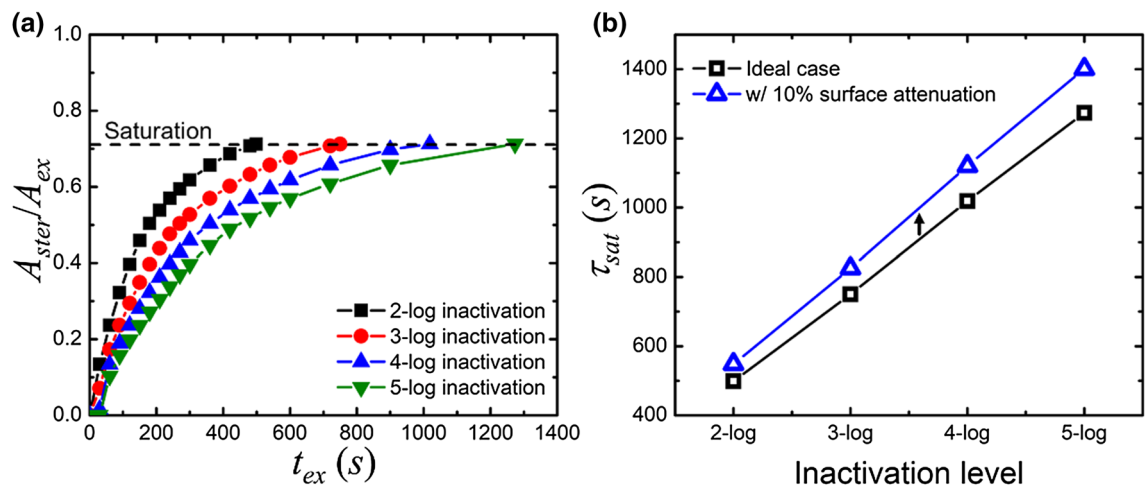


Figure 7. (a) Under different inactivation levels from 2-log to 5-log, A_{ster}/A_{ex} is a function of exposure time. A_{ster}/A_{ex} increases and gradually saturates around 0.71 where the exposure time is defined as saturation time τ_{sat} . (b) The effect of surface attenuation of UV-C radiation on the saturation time τ_{sat} is shown for inactivation levels from 2-log to 5-log.

τ_{sat} is directly proportional to the UV-C dose for effective sterilization. In this way, adopting the UVC LEDs with higher operating power can reduce the required τ_{sat} proportionally to realize the efficient sterilization. As shown in Fig. 7a, the required τ_{sat} increases with the level of inactivation. The material property¹⁹, superficial structure²⁸, and relative humidity²⁹ of the target surface may degrade the magnitude of SARS-CoV-2 inactivation. The superficial dirt in the food court is commonly due to edible oil stains. For example, a layer of chicken oil with a thickness of 0.34 mm can cause 10% and 8.5% attenuation of UV-C irradiance in 222 nm and 274 nm, respectively³⁰. In Fig. 7b, we evaluate τ_{sat} for the inactivation levels from 2-log to 5-log while assuming UV-C attenuation is 10% on the surface (i.e., $\eta = 0.1$). The increment of required τ_{sat} for the same inactivation level is simply proportional to τ_{sat} in the ideal case. If the UV-C light penetrates aerosols or encounters scattering and absorbing substances, we have to take into account the light extinction (i.e., $\alpha \neq 0$). For example, ozone has been commonly used for air disinfectants in which the concentration of ozone is even as high as 20 ppm³¹. In this case, the UV-C extinction due to ozone absorption at room temperature can be estimated and α is 0.6, 0.36, and 0.17 at the wavelength of 254, 274, and 222 nm, respectively³². Fig. 8a shows that τ_{sat} at $\alpha = 0.6$ is 3.9 times the ideal case. From Fig. 8b, we can deduce that τ_{sat} required for 274 and 222-nm UV-C sterilization increases to 2.2 and 1.5 times when assuming 20-ppm ozone in the air.

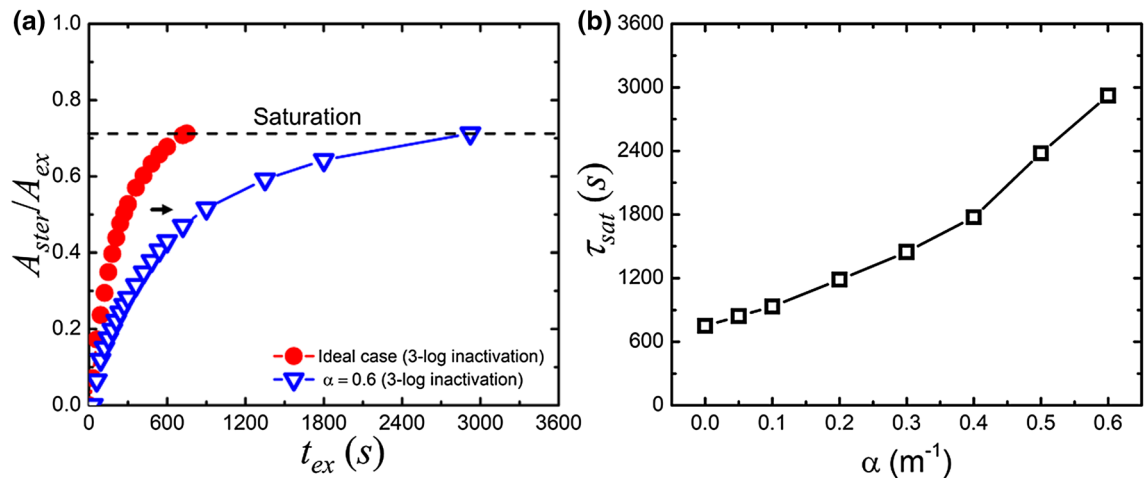


Figure 8. (a) The impact of extinction along the light path on the UV-C sterilization. (b) The saturation time τ_{sat} is a function of the extinction coefficient.

Conclusion

In conclusion, we have performed a feasibility study of UV-C LED for SARS-CoV-2 sterilization in the public environment using the ray-tracing (RT) solver. The proposed in-house RT simulator can generate various irradiance maps of a typical UV-C LED point source with a beam angle of 40°, 120°, and 160°. By linear superposition of individual LEDs, it is possible to realize the specific design of the LED array. The benchmark simulation of a LED strip has been conducted, and the results from the RT solver have good agreements with those from experimental measurements, the commercial software (Zemax OpticStudio), and the analytical solution. To evaluate the SARS-CoV-2 inactivation quantitatively, the values of the inactivation coefficient (K) has been derived from the proposed experimental data^{11,12}. According to the RT prediction of the irradiance profile of the emission from the germicidal system consisting of UV-C LEDs, we can clearly define the effective and safe zones in space and determine the optimised position to locate the UV-C germicidal system for the maximum area for the sterilization.

Moreover, a practical case study of a typical food court and the corresponding 3D UV-C irradiation mapping have been presented. From the predicted irradiation results, the viral inactivation map can be obtained. Based on the RT simulation results, the period (τ_{sat}) of saturation of the UV-C exposure can be defined as the minimum required time for effective sterilization. τ_{sat} is directly proportional to the required UV-C dose and rises as the inactivation level increases. For further analysis of the impact of environmental factors on the SARS-CoV-2 inactivation, the superficial effect and the substance in the air should be considered as they could potentially degrade the SARS-CoV-2 inactivation. These physical mechanisms have been modeled in the RT solver and τ_{sat} becomes longer as compared with the ideal case. The proposed example shows that τ_{sat} is expected to be 2.2 and 1.5 times longer for UV-C sterilization at the wavelengths of 274 and 222-nm when assuming 20-ppm ozone in the air. To summarize, according to RT simulations, we provide a useful guideline to improve the safety and efficiency of usage of the UV-C-LED-based germicidal system. Furthermore, our simulation approach can numerically optimise other UV germicidal systems' designs in different environmental settings and extend the model for airborne/aerosol ultra-violet germicidal irradiation (UVGI) disinfection applications. Based on a physically accurate and geometrically flexible RT technique, the proposed simulator will be effectively applied in the light-based inactivation, including the novel light source (e.g., VUV³³), on scenarios like aircraft cabins, hospitals, and shopping malls. In this case, the accurate experimental measurement of the corresponding environmental parameters η , α , and K versus the operating wavelength of the light source remains to be done.

Received: 23 June 2021; Accepted: 8 November 2021

Published online: 19 November 2021

References

1. Tang, S. *et al.* Aerosol transmission of SARS-CoV-2? Evidence, prevention and control. *Environ. Int.* **144**, 106039 (2020).
2. van Doremalen, N. *et al.* Aerosol and surface stability of SARS-CoV-2 as compared with SARS-CoV-1. *N. Engl. J. Med.* **382**(16), 1564–1567 (2020).
3. Ferretti, L. *et al.* Quantifying SARS-CoV-2 transmission suggests epidemic control with digital contact tracing. *Science* **368**, 619 (2020).
4. Li, D. & Sangion, A. Evaluating consumer exposure to disinfecting chemicals against coronavirus disease 2019 (COVID-19) and associated health risks. *Environ. Int.* **145**, 106108 (2020).
5. Pastorino, B., Touret, F., Gilles, M., Lamballerie, X. D. & Charrel, R. N. Heat inactivation of different types of SARS-CoV-2 samples: What protocols for biosafety, molecular detection and serological diagnostics?. *Viruses* **12**(7), 735 (2020).
6. Hadi, J., Dunowska, M., Wu, S. & Brightwell, G. Control measures for SARS-CoV-2: a review on light-based inactivation of single-stranded RNA viruses. *Pathogens* **9**(9), 737 (2020).
7. Raeiszadeh, M. & Adeli, B. A critical review on ultraviolet disinfection systems against COVID-19 outbreak: Applicability, validation, and safety considerations. *ACS Photonics* **7**, 2941–2951 (2020).

8. Kadama, A. R., Nairb, G. B. & Dholea, S. J. Insights into the extraction of mercury from fluorescent lamps: A review. *J. Environ. Chem. Eng* **7**, 103279 (2019).
9. Kneissl, M., Seong, T. Y., Han, J. & Amano, H. The emergence and prospects of deep-ultraviolet light-emitting diode technologies. *Nat. Photonics* **13**, 233–244 (2019).
10. Buchan, A. G., Yang, L. & Atkinson, K. D. Predicting airborne coronavirus inactivation by far-UVC in populated rooms using a high-fidelity coupled radiation-CFD model. *Sci. Rep.* **10**, 19659 (2020).
11. Buonanno, M., Welch, D., Shuryak, I. & Brenner, D. J. Far-UVC light (222 nm) efficiently and safely inactivates airborne human coronaviruses. *Sci. Rep.* **10**, 10285 (2020).
12. Minamikawa, T. *et al.* Quantitative evaluation of SARS-CoV-2 inactivation using a deep ultraviolet light-emitting diode. *Sci. Rep.* **11**, 5070 (2021).
13. Inagaki, H., Saito, A., Sugiyama, H., Okabayashi, T. & Fujimoto, S. Rapid inactivation of SARS-CoV-2 with deep-UV LED irradiation. *Emerg. Microbes Infect.* **9**, 1744–1747 (2020).
14. Ong, Q. *et al.* Irradiation of UVC LED at 277 nm inactivates coronaviruses by photodegradation of spike protein. *bioRxiv* <https://doi.org/10.1101/2021.05.31.446403> (2021).
15. Liu, S. *et al.* Sec-eliminating the SARS-CoV-2 by AlGaN based high power deep ultraviolet light source. *Adv. Funct. Mater.* **31**, 2008452 (2021).
16. Documentation of the Threshold Limit Values[®] and Biological Exposure Indices, in *8th Edition, Cincinnati: American Conference of Governmental Industrial Hygienists (ACGIH)* (2021).
17. International Commission on Non-Ionizing Radiation Protection (ICNIRP). Guidelines on limits of exposure to ultraviolet radiation of wavelengths between 180 and 400 nm (incoherent optical radiation). *Health Phys.* **87**(2), 171–186 (2004).
18. Hou, M., Pantelic, J. & Aviv, D. Spatial analysis of the impact of UVGI technology in occupied rooms using ray-tracing simulation. *Indoor Air* **31**(5), 1625–1638 (2021).
19. Gidari, A. *et al.* SARS-CoV-2 survival on surfaces and the effect of UV-C light. *Viruses* **13**(3), 408 (2021).
20. Moreno, I. & Sun, C. C. Modeling the radiation pattern of LEDs. *Opt. Express* **16**, 1808 (2008).
21. Kheyrandish, A., Taghipour, F. & Mohseni, M. UV-LED radiation modeling and its applications in UV dose determination for water treatment. *J. Photochem. Photobiol. A* **352**, 113–121 (2018).
22. "OpticStudio 20.1," Zemax, LLC, Kirkland. www.zemax.com. Washington, United States (2020).
23. DIN 5031-10:1979-11. *Strahlungsphysik im optischen Bereich und Lichttechnik*. (Withdrawn, Updated Version: DIN 5031-10:2000-03) (Deutsches Institut für Normung, 1979).
24. IESNA. *IESNA Lighting Handbook* 9th edn. (Illuminating Engineering Society of North America, 2000).
25. Hasan, M. & Lee, M. Enhancement of the thermo-mechanical properties and efficacy of mixing technique in the preparation of graphene/PVC nanocomposites compared to carbon nanotubes/PVC. *Prog. Nat. Sci.: Mater. Int.* **24**(6), 579–587 (2014).
26. Rico, V. J. *et al.* Laser treatment of nanoparticulated metal thin films for ceramic tile decoration. *ACS Appl. Mater. Interfaces* **8**, 24880–24886 (2016).
27. National Environment Agency, *Safety Guidelines for Use of UVC Devices in Commercial/Industrial Settings*. <https://www.nea.gov.sg/our-services/radiation-safety/safety-guidelines-for-use-of-uvc-devices>. (2021).
28. Zhao, Z. *et al.* Germicidal ultraviolet light does not damage or impede performance of N95 masks upon multiple uses. *Environ. Sci. Technol. Lett.* **7**, 600–606 (2020).
29. Kowalski, W. *Ultraviolet Germicidal Irradiation Handbook* (Springer, 2009).
30. Anil Kumar, K. & Viswanathan, K. Study of UV transmission through a few edible oils and chicken oil. *J. Spectrosc. (Hindawi)* <https://doi.org/10.1155/2013/540417> (2013).
31. Grignani, E. *et al.* Safe and effective use of ozone as air and surface disinfectant in the conjuncture of Covid-19. *Gases* **1**(1), 19–32 (2021).
32. Gorshelev, V., Serdyuchenko, A., Weber, M., Chehade, W. & Burrows, J. P. High spectral resolution ozone absorption cross-sections—Part 1: Measurements, data analysis and comparison with previous measurements around 293 K. *Atmos. Meas. Tech.* **7**, 609–624 (2014).
33. Szeto, W., Yam, W. C., Huang, H. & Leung, D. Y. The efficacy of vacuum-ultraviolet light disinfection of some common environmental pathogens. *BMC Infect. Dis.* **20**, 127 (2020).

Acknowledgements

We would like to acknowledge the funding support from A*STAR Enterprise for the project "A*CRUSE-UV LED for Disinfection studies" (Ref. no. : ACCL/19-GAP064-R20A-0, GAP/2020/00392).

Author contributions

P.Y.L., H.L., and R.J.H.N. conducted the simulations. P.Y.L. wrote the manuscript. P.Y.L., H.L., and R.J.H.N. interpreted and organized data. B.W.H.T. prepared input files for simulations. H.S.C. and C.E.P. initiated and advised the study. J.W.R.T., Q.O., and Y.L. conceived and conducted the experiments. All authors reviewed the manuscript.

Competing interests

The authors declare no competing interests.

Additional information

Correspondence and requests for materials should be addressed to P.-Y.L.

Reprints and permissions information is available at www.nature.com/reprints.

Publisher's note Springer Nature remains neutral with regard to jurisdictional claims in published maps and institutional affiliations.



Open Access This article is licensed under a Creative Commons Attribution 4.0 International License, which permits use, sharing, adaptation, distribution and reproduction in any medium or format, as long as you give appropriate credit to the original author(s) and the source, provide a link to the Creative Commons licence, and indicate if changes were made. The images or other third party material in this article are included in the article's Creative Commons licence, unless indicated otherwise in a credit line to the material. If material is not included in the article's Creative Commons licence and your intended use is not permitted by statutory regulation or exceeds the permitted use, you will need to obtain permission directly from the copyright holder. To view a copy of this licence, visit <http://creativecommons.org/licenses/by/4.0/>.

© The Author(s) 2021